Journal of Aerosol Science 129 (2019) 116–123

Contents lists available at ScienceDirect

Journal of Aerosol Science

journal homepage: www.elsevier.com/locate/jaerosci

Fluctuation-theorem method of measuring a particle's mass without knowing its shape or density

Chun-Shang Wong[a,*], Ranganathan Gopalakrishnan[b], J. Goree[a]

[a] Department of Physics and Astronomy, University of Iowa, Iowa City, IA, United States
[b] Department of Mechanical Engineering, University of Memphis, Memphis, TN, United States

ARTICLE INFO

Keywords:
Aerosol particle
Mass measurement
Fluctuation theorem
Brownian motion
Settling velocity

ABSTRACT

Tracking the Brownian motion of aerosol particles as they settle in air allows a mass measurement. The particle typically falls downward at its terminal settling velocity; however, the particle occasionally will be displaced upwards due to Brownian fluctuations. The number of occurrences of upward and downward fluctuations is compared, using the formula for the work fluctuation theorem, to yield the mass. This method can be applied to either a single particle or a collection of particles. The advantages of this method include no required information about the size, shape, or density of the particle. Details of the analysis method are presented and illustrated with experimental data.

1. Introduction

The combined effects of fluctuating Brownian motion and steady terminal-velocity motion allow a measurement of particle mass, presented in this paper. In the force field of gravity alone, for a sufficiently small particle, the settling velocity diminishes enough that Brownian fluctuations can become prominent. Occasionally, the Brownian movements will briefly overcome the settling velocity, so that a particle's velocity can completely change sign. A free-falling particle can briefly be displaced “upwards” against the downward field of gravity. This motion against the force causing the drift can be interpreted as negative work done by the field on the particle, or an extraction of energy by the particle from the field. Such negative work extraction by the particle happens with a definite probability, predicted by the work fluctuation theorem (van Zon & Cohen, 2003). This theorem forms the basis of the mass measurement technique we report here.

In a previous communication (Wong, Goree, & Gopalakrishnan, 2018), we experimentally demonstrated the technique, using simple equipment including a settling chamber and a high-resolution video camera. By observing the trajectories of individual particles, histograms were constructed for the vertical displacements as particles fell under gravity. These histograms were then used to directly measure a mass for the falling particle, using the formula of the work fluctuation theorem. Advantages of this method, as described in Ref. Wong et al. (2018), include a simple apparatus, and an analysis method that requires no information about the particle's shape, density, or electric charge.

In this article, we present further details of the mass measurement method, with an emphasis on the practical implementation. We define the requirements that the apparatus must meet. We then list the analysis steps, which we illustrate in a step-by-step example using experimental data from our previous communication (Wong et al., 2018), using standard particles. We also discuss the factors that limit the mass range that can be accurately measured using this technique, and how they can be overcome with an enhanced

* Correspondence to: Sandia National Laboratories, Livermore, CA 94551, United States.
E-mail address: chuwong@sandia.gov (C.-S. Wong).

https://doi.org/10.1016/j.jaerosci.2018.12.009
Received 14 September 2018; Received in revised form 5 December 2018; Accepted 23 December 2018
Available online 26 December 2018
0021-8502/

design for the instrument.

2. Previous mass measurement methods

Mass plays such a prominent role in aerosol transport that many methods have been devised to obtain its value. We review many of these previous methods here.

One common approach to measure the mass of *individual* particles or the mass distribution of an aerosol population is integral detectors coupled to a classification mechanism. The classification mechanism separates particles based on a specific interaction with gas and/or external fields. These methods mainly are used to observe the aggregate effects of an aerosol particle population (Kulkarni et al., 2011). For instance, various online measurement techniques such as light scattering (Mulholland et al., 2013), differential mobility analysis (Hagen & Alofs, 1983; Knutson & Whitby, 1975a, 1975b; Wang & Flagan, 1990), diffusion battery methods (Sinclair, 1972; Sinclair, Countess, Liu, & Pui, 1976) and offline techniques such as electron microscopy are used to measure aerosol particle size distribution $n(d_p)$. From the size distribution $n(d_p)$, the mass distribution $n(m_p)$ or its moments (average $\bar{m}$ and variance $\bar{m}^2$) are *inferred*, rather than precise measurements of the mass of individual particles. The inference of the mass distribution of an aerosol from a measured size distribution $n(d_p)$, although quite common, requires assumptions pertaining to the density (composition) and the morphology of measured particles. The measured "size" corresponds to either an interaction size such as the aerodynamic diameter, diffusion diameter, mobility diameter, sedimentation diameter or a geometric size inferred from electron microscopy. The mass distribution of the aerosol $n(m_p) = \rho d_p^3 n(d_p)$ can be obtained in a straightforward manner if the shape and density of the particles are known or suitably assumed. These limitations of detectors based on classification mechanisms can be avoided using the new method described in this article.

Aerosol particles are not always spherical, so that it is desirable to have a mass measurement method that is independent of shape, like our method. While aerosols generated under homogenous residence times in a growth environment (exposure to concentration of condensing vapor and temperature history) develop into a nearly spherical shape and uniform composition (Feng et al., 1994), non-spherical particles with variable chemical composition and density are more common in atmospheric as well synthetic environments.

Previous methods with capabilities close to ours, for the measurement of the mass distribution of aerosols without assumptions about their shape or density, are the aerosol particle mass analyzer developed by Ehara and co-workers (Ehara, Hagwood, & Coakley, 1996) and the centrifugal particle mass analyzer developed by Olfert and co-workers (Olfert & Collings, 2005). These instruments introduce charged aerosol particles in the electric field that exists in the annular space between two cylinders rotating with respect to each other. The electric force and the centrifugal force on the particle are balanced by adjusting the rotation speed and applied voltage to infer the mass to charge ratio of the particles. By introducing particles of known charge state, the aerosol particle mass analyzer measures the mass distribution of an aerosol population without reference to a shape or density (Liao, Tseng, & Tsai, 2017; Lin et al., 2014; Tajima, Sakurai, Fukushima, & Ehara, 2013). When combined with electrical mobility analysis (Buckley, Kimoto, Lee, Fukushima, & Hogan, 2017; Chen, Ghosh, Buckley, Sankaran, & Hogan, 2018; Geller, Biswas, & Sioutas, 2006; Lall, Ma, Guha, Mulholland, & Zachariah, 2009; Lee, Widiyastuti, Tajima, Iskandar, & Okuyama, 2009; Malloy et al., 2009), the aerosol and centrifugal particle mass analyzers have also been used to measure the two-dimensional size and mass distributions of different types of aerosols. The aerosol particle mass analyzer requires information about the charge state or charge distribution of the aerosol being measured. The charge of ambient and laboratory aerosols are often conditioned by exposing the particles to bipolar ions of approximately equal concentration in aerosol chargers. This allows the particles to attain a steady-state charge, size-dependent charge distribution. For particles $<0.5\,\mu$m the charge distribution can be calculated using bipolar charging models (Gopalakrishnan, Meredith, Larriba-Andaluz, & Hogan, 2013; Wiedensohler, 1988). For particles $\geq 0.5\,\mu$m the charge distribution is commonly assumed to have a Boltzmann profile (Gunn, 1954, 1955). Typically, a differential mobility analyzer is used upstream of the aerosol particle mass analyzer to introduce particles of known mobility (charge state and size), thereby making the inference of mass distribution possible (Scheckman, McMurry, & Pratsinis, 2009). For aerosols of unknown charge distributions, the instrument yields the mass to charge ratio (Ehara et al., 1996).

3. Analysis method

3.1. Analysis steps to obtain the mass m_i of a single particle

Our fluctuation-theorem mass measurement requires, most importantly, a time series of vertical positions $y_i(t)$ of particle i. In addition, it requires the air temperature T and the gravitational constant g. (The apparatus and measurement method for obtaining such a time series is discussed later, in Section 4.) From these inputs, the mass m_i of particle i, can be obtained by choosing a value of τ and following these seven steps.

(1) First, divide the time series data $y_i(t)$ of particle i into non-overlapping time segments of duration τ.
(2) Second, compute the vertical displacement $\Delta y_{\tau,i} = y_i(t+\tau) - y_i(t)$ of particle i. This is repeated for each time segment.
(3) Third, prepare a histogram by binning the computed values of the vertical displacement $\Delta y_{\tau,i}$. The bins of the histogram are equally spaced and non-overlapping. We will use the symbol C to represent the value of $\Delta y_{\tau,i}$ at the center of the bin. One can choose any positive value of C; it will correspond to another bin at $-C$. A histogram bin's count, $p(\Delta y_{\tau,i} = C)$, is the number of observations of $\Delta y_{\tau,i}$ that fall within the bin centered at $\Delta y_{\tau,i} = C$.
(4) Fourth, using data from the histogram, compute

$$\ln R = \ln\left[\frac{p(\Delta y_{\tau,i} = C)}{p(\Delta y_{\tau,i} = -C)}\right], \tag{1}$$

which we will term the displacement-count ratio. Each pair of counts in the histogram for bins centered at + C and − C yields one value of ln R. The displacement-count ratio is computed not for just one value of C, but for a wide range of values of C.

(5) Fifth, plot the obtained values of the displacement-count ratio ln R as the vertical axis of a graph, with the bin value C as the horizontal axis.

(6) Sixth, fit the plotted displacement-count ratio ln R to a straight line to obtain the slope s_i, for individual particle i.

(7) Seventh, compute the mass m_i of the individual particle as

$$m_i = -\left(\frac{k_B T}{g}\right) s_i, \tag{2}$$

which also requires the air temperature T, the Boltzmann constant $k_B = 1.38 \times 10^{-23}$J/K, and the gravitational constant g. Precise values of g for geographic locations are tabulated in standard references (Pavlis, Holmes, Kenyon, & Factor, 2008).

Optionally, the step-by-step procedure above can be repeated with different choices of the parameter τ. For each value of τ, one will obtain one measurement of m_i. All of these measurements can be averaged, if desired, to improve statistics.

This method can also be used to obtain the mass distribution $n(m_i)$ of a population of particles. Obtaining $n(m_i)$ requires time series of vertical positions for N particles belonging to the particle population. Then, simply repeating this procedure for each of the N time series will yield a sample of the mass distribution of the particle population. Practically speaking, if the particles are relatively monodisperse, a sample size of approximately $N = 100$ should be sufficient to yield accurate estimates of $n(m_i)$.

Detailed derivations of the equations used in this section are provided in Appendix B.

3.2. Extension of method to obtain the average mass m_{avg} of many particles

Instead of the mass of a single particle m_i, one can instead obtain the average mass m_{avg} of N particles, if all the particles have a similar mass. The input data required are time series of vertical positions $y_i(t)$ for each of the N particles. The steps for obtaining m_{avg} are nearly identical to the steps provided in Section 3.1 above, but with a few minor changes as listed below.

Steps (1) and (2) are repeated for each of the N particles and their position time series $y_i(t)$.

In step (3), the histogram is built for data combined for all N particles.

Step (6) will yield a slope s_{avg}, based on a single graph of data.

For step (7), Eq. (2) is

$$m_{\text{avg}} = -\left(\frac{k_B T}{g}\right) s_{\text{avg}}. \tag{3}$$

When obtaining the average mass m_{avg} of many particles it is typically optimal to combine the histogram data of vertical displacements $\Delta y_{\tau,i}$ before computing the displacement-count ratio ln R and finding its slope s_{avg}, as opposed to computing ln R and s for each particle and averaging the slopes to obtain s_{avg}. This suggested sequence of steps helps minimize the finite-size effects in the histogram counts, since upward displacements can be rare when a single particle is tracked for a short time.

3.3. Example of analysis method

Here we present a step-by-step analysis of experimental data, using the steps provided in Sections 3.1 and 3.2. The data are from our demonstration experiment, which we reported in Ref. Wong et al. (2018). We start with position time series data for $N = 69$ particles. Sample time series of particle positions are shown in Fig. 1. The vertical motion of the particles, in Fig. 1(a), is mostly a downward trend that corresponds to a terminal settling velocity. On occasion, the particles are displaced upward against the force of gravity due to Brownian motion, as shown in the inset. Observations of these upward fluctuations are crucial for our mass measurement method. Details of the demonstration-experiment apparatus are provided in the Section 4.2.

We began by choosing a time duration $\tau = 25$ ms. For step (1), the position time series $y_i(t)$ of each particle i was divided into 25 ms intervals. Next, for step (2) we compute the vertical displacement $\Delta y_{\tau,i} = y_i(t + \tau) - y_i(t)$ for each of the time segments, which yields 40, 870 observations of $\Delta y_{\tau,i}$. For step (3), we bin and count the observations of $\Delta y_{\tau,i}$ to produce the histogram presented in Fig. 2(a).

For step (4), we choose a pair of bins from the histogram that are centered at the value $\Delta y_{\tau,i} = C$ and the corresponding value $\Delta y_{\tau,i} = -C$. The counts within these bins are used as the input for Eq. (1) to compute a single value of the displacement-count ratio ln R. We repeat this process for all pairs of bins in the histogram; one example pair of histogram bins, and the corresponding computed value of ln R, is indicated by arrows in Fig. 2.

For step (5), we prepare a graph with the obtained values of the displacement-count ratio ln R as the vertical axis, and the histogram bin value C as the horizontal axis. This graph is presented in Fig. 2(b). We next, for step (6), fit a straight line through the plotted values of ln R, yielding the slope $s_{\text{avg}} = -1.94\ \mu\text{m}^{-1}$.

For step (7), we use Eq. (3) to obtain the average mass $m_{\text{avg}} = 8.073 \times 10^{-16}$kg for the $N = 69$particles. The inputs for the

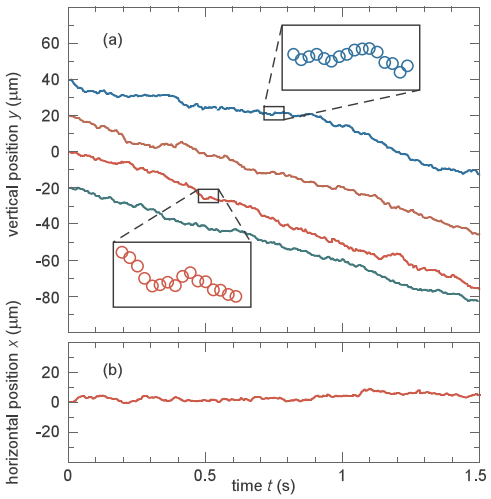

Fig. 1. Example time series data of particle positions from our demonstration experiment. While the particles typically fell downwards at the terminal settling velocity as indicated by the general trend, they occasionally had upward displacements against the force of gravity, as highlighted in the insets. The sampling rate of our data was chosen so that there were multiple data points in the upward displacements seen here. Data shown are for four particles; their graphs are displaced vertically for clarity. This figure is a reproduction of Fig. 2 from Wong et al. (2018).

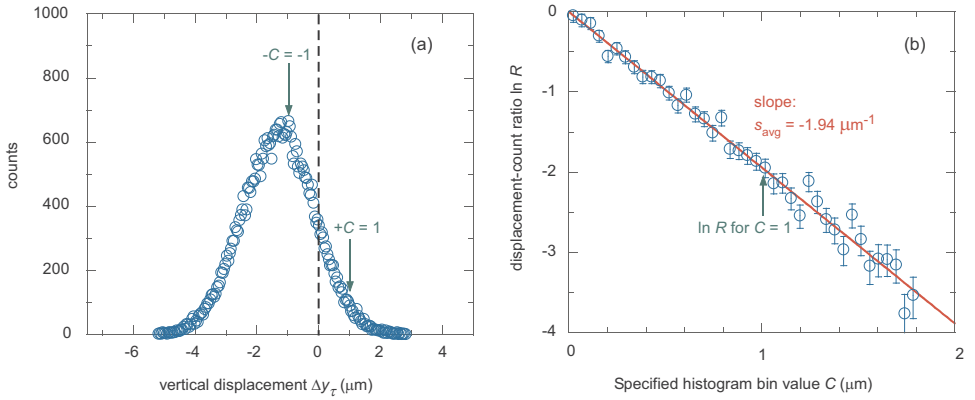

Fig. 2. (a) Histogram of vertical displacements $\Delta y_{\tau,i}$ for 69 particles. In analysis step (4), we choose a value C, and thereby choose a pair of histogram bins for $\Delta y_{\tau,i} = +C$ and $\Delta y_{\tau,i} = -C$, as indicated by arrows in (a). Next, Eq. (1) is computed from counts within the histogram bins for $+C$ and $-C$. We repeat this for many choices of C. In step (5), we plot the displacement-count ratio $\ln R$ in (b). In step (6), we fit the data points in (b) to a straight line through the origin, yielding the slope s_{avg}, which was used in Eq. (2) to compute the average mass of the 69particles.

calculation include $s = -1.94\,\mu\text{m}^{-1}$, $g = 9.804\text{m/s}^2$, $T = 295\text{K}$, and $k_B = 1.38 \times 10^{-23}\text{J/K}$.

For this demonstration, we choose to perform the optional ave'raging, repeating steps (1)-(7) for multiple values of the specified time duration τ. We choose six values of τ in the range of 30 ms to 55 ms. Each value of τ yields a separate mass measurement, which we average to decrease the size of error bars, yielding our final mass measurement $m_{\text{avg}} = (8.07 \pm 0.10) \times 10^{-16}\text{kg}$ for the 69 particles that we analyzed.

For comparison, we obtained a reference mass measurement of $m_{\text{avg}} = (8.13 \pm 0.11) \times 10^{-16}\text{kg}$ for the $N = 69$particles, which agrees within error bars with our fluctuation-theorem-method measurement. This reference measurement had the limitation that it requires particles to be spherical (unlike the fluctuation-theorem method, which places no constraints on particle shape). The inputs for the reference mass measurement were the particles' terminal settling velocity and average horizontal diffusion coefficient, as well as the air temperature T and gravitational constant g.

4. Apparatus

4.1. Requirements

A simple implementation of the mass measurement method is possible, with only two main requirements. The *force requirement* is that the particle must undergo free-fall with no disturbing forces other than gravity. In the simplest case, the particle will fall in still air to avoid wind-like forces. The *tracking requirement* is that the particle's vertical motion must be observed to yield a position time

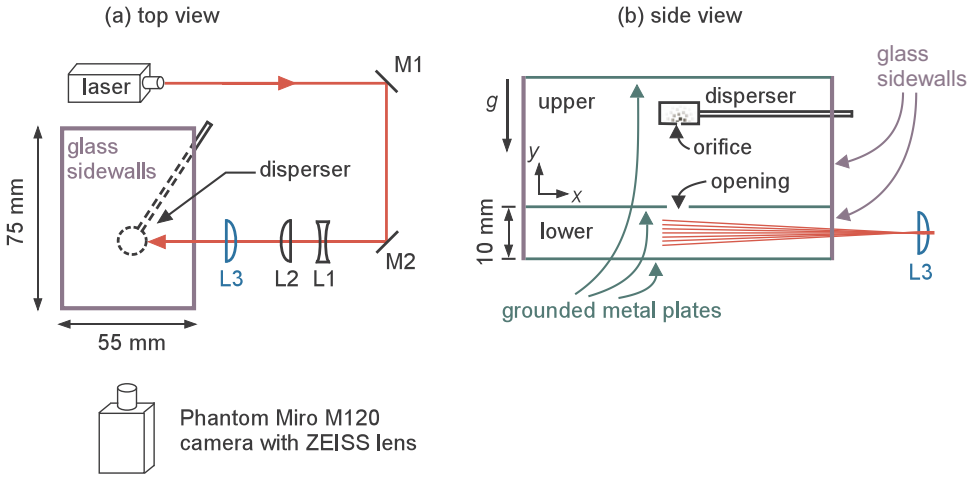

Fig. 3. Sketch of the demonstration-experiment apparatus, as viewed from the (a) top and (b) side. The *force requirement* was met by the glass walls and grounded metal plates that eliminated air currents and stray electric fields. The *tracking requirement* was met by imaging particles with a video camera. A 15-mW HeNe laser beam was shaped to illuminate falling particles within a vertical cross section of the lower chamber. The optics used for the illumination, not drawn to scale, include: mirrors M1 and M2, spherical lenses L1 and L2, and cylindrical lens L3. A thermometer, not shown here, recorded the room temperature. This figure is a reproduction of Figs. 1(a) and (b) from Wong et al. (2018).

series $y_i(t)$. This tracking can be done with a video camera and image-analysis software. Additionally, the air temperature T and the gravitational constant g are required.

4.2. Design for demonstration experiment

A two-chamber apparatus, shown in Fig. 3, was used in our demonstration experiment. Particles were dropped from the disperser in the upper chamber, and fell through a 6-mm diameter opening into the lower chamber. This apparatus has a simple design, without any powered electrodes, instruments for electric charging of particles, or power supplies to exert forces on the particle.

To meet the *force requirement*, the two-chamber design minimized convection currents in the lower chamber. To accomplish this, the lower chamber had a small height so that any temperature gradient is unlikely to cause the critical Rayleigh number to be exceeded. Furthermore, the top and bottom walls of the chambers were grounded to eliminate disturbing electric fields.

To meet the *tracking requirement*, particles were illuminated by a sheet of laser light and imaged by a side-view video camera within the lower chamber. The camera was a Phantom Miro M120 that imaged at 200 frames/s. The image-analysis software that was used was ImageJ (Feng, Goree, & Liu, 2007) This setup for illumination and imaging was adequate to track micron-sized particles.

The particles that we used in the demonstration experiment were polymer (melamine formaldehyde) and were nominally 1.04 μm

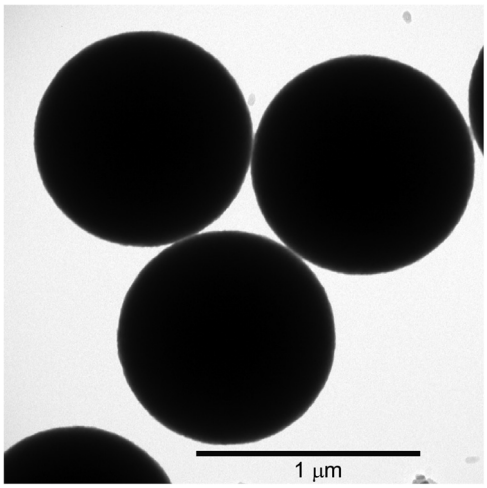

Fig. 4. Particles from the same bottle as used in our demonstration experiment imaged with a transmission electron microscope. The spherical shape of the particles is not necessary for the fluctuation-theorem mass measurement method. This figure is a reproduction of Supplemental Fig. 1 from Ref. Wong et al. (2018).

in diameter according to the manufacturer's specifications. Particles were confirmed to be spherical, Fig. 4.

4.3. Approach for incorporating the method in a continuous flow system

Continuous flow systems with multiple devices are often used to sample, measure, and transport aerosols. It may be attractive to couple the fluctuation-theorem mass measurement method with other measurement systems, such as differential mobility analyzers or diffusion batteries.

We suggest one possible implementation here. A gas containing the particles can be flowed through a measurement volume, where individual particles are tracked using video cameras to yield time series of their vertical positions, as in our demonstration experiment. The gas flow is required to be steady and laminar, so that its effect on a particle motion can be completely characterized and, if necessary, removed. For example, if the flow has a vertical component, then the constant displacement that a particle experiences due to the flow must be subtracted from the particle's vertical positions. On the other hand, if the gas flow is entirely horizontal (perpendicular to the gravitational force), then no changes to the analysis steps would be required.

4.4. Design for an extended mass measurement range

Our mass measurement method worked well with data from our demonstration experiment for 1-micron particles. Smaller particles could in principle be measured using exactly the same method. The only challenge for smaller particles is obtaining sufficient light scattering, for tracking.

For larger particles, we can propose an enhancement to the apparatus. The problem that must be avoided, with large particles, is that they will fall too fast with too few upward displacements. This problem can be remedied by changing either the accelerating field or the damping force. In our demonstration experiment, the accelerating field was simply a 1-g gravitational acceleration, and the damping force was gas drag at atmospheric pressure.

We can reduce the accelerating field by adding an electric force that opposes gravity. This approach requires applying a known charge q_i to each particle, and it also requires electrodes to apply a uniform electric field throughout the measurement volume. In this approach, Eq. (2) becomes

$$m_i = -\left(\frac{k_B T}{g}\right) s - \frac{q_i E}{g}. \tag{4}$$

By increasing the air pressure, one can reduce the settling velocity. In this way, the observation time is increased so that the number of observations of upward displacement is adequate. The analysis procedure and formulas would be the same as in Section 3.1.

5. Choosing τ

Minimizing the uncertainty of the mass measurement relies on improving the counting statistics for the histogram of $\Delta y_{\tau,i}$. In particular, the histogram should have a large number of counts for upward displacements. Parameters in the experiment and analysis can be chosen to provide the best conditions for observing a sufficient number of these upward displacements. Here, we discuss the choice of the specified time interval τ.

An appropriate value for τ can be determined by examining the experimental data. The main requirement is that the histogram should include a significant number of upward displacement events. As a starting point, one can vary τ until the histogram's mean value and half-width are comparable, which typically occurs when $-mgv_{i,\mathrm{term}}\tau \approx kT$. Here $v_{i,\mathrm{term}}$ is the terminal settling velocity of particle i.

Since one obtains a measurement of mass for each value of τ, it can be desirable to repeat the measurement analysis for several values of τ, as discussed above in Section 3.1. The measured masses can be averaged to help improve statistics, and the variations in the measured masses can help quantify the measurement uncertainty.

Besides the factors mentioned above, which center on statistics, in an extreme case one could encounter a physical limitation in the method by choosing too short a value of τ. This physical limitation concerns the asymptotic-limit requirement of the fluctuation theorem (Wong, Goree, Haralson, & Liu, 2017). A possible symptom of this problem would be a detectable trend in the data for mass measurement vs τ.

Acknowledgements

We thank R. Belousov for helpful discussions. Work at the University of Iowa was supported by the US National Science Foundation Award 11626451162645, US Department of Energy Grant DE-SC0014566, Army Research Office award W911NF1810240 Subaward No. A006827502, and NASA Subcontract 1562068.

Appendix A. Impact of air temperature and pressure on mass measurement

The air within the apparatus acts as a thermal bath for particles that are falling through it. The air temperature T affects the size of

fluctuations in particle motion; a higher T leads to larger random particle displacements, and likewise, a lower T leads to smaller random particle displacements. In particular, a higher T may be helpful when measuring the mass of larger particles that may otherwise have fluctuations too small to resolve.

Errors associated with air temperature T are most likely associated to either a systematic error in the measured T or air currents driven by temperature gradients. First, a systematic error in the measured T leads to a proportionally sized error in the measured mass, as can be seen by inspecting Eq. (2). For example, a 1% systematic error in temperature (approximately 3 K at room temperature) would lead to a 1% error in the measured mass. Second, air currents driven by temperature gradients can do work on an otherwise free-falling particle, so that the method may no longer be applicable. Precautions in the apparatus design should be taken to minimize temperature gradients or their effects (such as the chamber height consideration discussed in Section 4.2).

The air pressure within the apparatus affects not only the size of fluctuations in particle motion, but also the terminal settling velocity. Higher air pressures lead to smaller fluctuations and slower settling velocities, while lower air pressures lead to larger fluctuations and faster settling velocities. Conveniently, these air-pressure effects cancel out when using the fluctuation-theorem method, so that the resulting mass measurement is independent of air pressure (i.e. air pressure does not enter any equation used in the method). Since the fluctuation-theorem method is valid at any pressure, the air pressure should be chosen to optimize particle motion to allow for precise tracking. In particular, the video cameras must be able to resolve the size and duration of upward displacements of particles.

Appendix B. Derivations

Here we provide derivations of Eqs. (1) and (2).

For a particle i undergoing free fall due to gravity, the work $W_{\tau,i}$ done during a time interval τ is given by

$$W_{\tau,i} = -m_i g \Delta y_{\tau,i}. \tag{B.1}$$

This quantity can be normalized by $k_B T$ to yield the normalized work,

$$w_{\tau,i} = -\frac{m_i g \Delta y_{\tau,i}}{k_B T}. \tag{B.2}$$

The work fluctuation theorem of van Zon and Cohen (2003) predicts that the normalized work w_τ will obey

$$\ln\left[\frac{p(w_{\tau,i} = -C')}{p(w_{\tau,i} = C')}\right] = -C', \text{ as} \tau \to \infty\ . \tag{B.3}$$

To implement this formula using experimental data, $p(w_{\tau,i} = C')$ is the number of counts in a histogram of observations of $w_{\tau,i}$. In particular, p is the number of counts within a histogram bin centered at C'. Substituting Eq. (B.2) into the left-hand side of Eq. (B.3) yields

$$\ln\left[\frac{p\left(-\frac{m_i g \Delta y_{\tau,i}}{k_B T} = -C'\right)}{p\left(-\frac{m_i g \Delta y_{\tau,i}}{k_B T} = C'\right)}\right] = -C', \text{ as} \tau \to \infty\ . \tag{B.4}$$

The limit $\tau \to \infty$ requires, in practice, a value of τ large enough to achieve a convergence of the two sides of this equation. Such a convergence time requires an adequate number of stochastic fluctuations, for example due to Brownian motion. Substituting a chosen value

$$C' = C\frac{m_i g}{k_B T} \tag{B.5}$$

in Eq. (B.4) gives

$$\ln\left[\frac{p(\Delta y_{\tau,i} = C)}{p(\Delta y_{\tau,i} = -C)}\right] = \frac{m_i g\ C}{k_B T}, \text{ as} \tau \to \infty\ , \tag{B.6}$$

which we can write as LHS = RHS.

Finally, we see that the mass m_i can be obtained from the derivative $d(\text{LHS})/\text{dC}$. This result leads us to the prescription of steps (6) and (7) of our procedure. The mass m_i is found from the slope s_i of a graph of the LHS vs C.

References

Buckley, D. T., Kimoto, S., Lee, M.-H., Fukushima, N., & Hogan, C. J. (2017). Technical note: A corrected two dimensional data inversion routine for tandem mobility-mass measurements. *Journal of Aerosol Science, 114*, 157–168. https://doi.org/10.1088/1361-6463/aad26f.

Chen, X., Ghosh, S., Buckley, D. T., Sankaran, R. M., & Hogan, C. J. (2018). Characterization of the state of nanoparticle aggregation in non-equilibrium plasma synthesis systems. *Journal of Physics D: Applied Physics, 51*(*33*), 335203. https://doi.org/10.1016/j.jaerosci.2017.09.012.

Ehara, K., Hagwood, C., & Coakley, K. J. (1996). Novel method to classify aerosol particles according to their mass-to-charge ratio-aerosol particle mass analyser. *Journal of Aerosol Science, 27*(*2*), 217–234. https://doi.org/10.1016/0021-8502(95)00562-5.

Feng, J., Biskos, G., & Schmidt-Ott, A. Toward industrial scale synthesis of ultrapure singlet nanoparticles with controllable sizes in a continuous gas-phase process. *Scientific Reports 5* (1). doi:10.1038/srep15788.

Feng, Y., Goree, J., & Liu, B. (2007). Accurate particle position measurement from images. *Review of Scientific Instruments, 78*(*5*), 053704. https://doi.org/10.1063/1.2735920.

Geller, M., Biswas, S., & Sioutas, C. (2006). Determination of particle effective density in urban environments with a differential mobility analyzer and aerosol particle mass analyzer. *Aerosol Science and Technology, 40*(*9*), 709–723. https://doi.org/10.1080/02786820600803925.

Gopalakrishnan, R., Meredith, M. J., Larriba-Andaluz, C., & Hogan, C. J. (2013). Brownian dynamics determination of the bipolar steady state charge distribution on spheres and non-spheres in the transition regime. *Journal of Aerosol Science, 63*, 126–145. https://doi.org/10.1016/j.jaerosci.2013.04.007.

Gunn, R. (1954). Diffusion charging of atmoospheric droplets by ions, and the resulting combination coefficients. *Journal of Meteorology, 11*(*5*), 339–347 (doi:10.1175/1520-0469)(1954)(011 < 0339:dcoadb > 2.0.co;2).

Gunn, R. (1955). The statistical electrification of aerosols by ionic diffusion. *Journal of Colloid Science, 10*(*1*), 107–119. https://doi.org/10.1016/0095-8522(55)90081-7.

Hagen, D. E., & Alofs, D. J. (1983). Linear inversion method to obtain aerosol size distributions from measurements with a differential mobility analyzer. *Aerosol Science and Technology, 2*(*4*), 465–475. https://doi.org/10.1080/02786828308958650.

Knutson, E., & Whitby, K. (1975a). Aerosol classification by electric mobility: Apparatus, theory, and applications. *Journal of Aerosol Science, 6*(*6*), 443–451. https://doi.org/10.1016/0021-8502(75)90060-9.

Knutson, E., & Whitby, K. (1975b). Accurate measurement of aerosol electric mobility moments. *Journal of Aerosol Science, 6*(*6*), 453–460. https://doi.org/10.1016/0021-8502(75)90061-0.

Kulkarni, P., Baron, P. A., & Willeke, K. (Eds.). (2011). *Aerosol Measurement*John Wiley & Sons, Inc.https://doi.org/10.1002/9781118001684.

Lall, A. A., Ma, X., Guha, S., Mulholland, G. W., & Zachariah, M. R. (2009). Online nanoparticle mass measurement by combined aerosol particle mass analyzer and differential mobility analyzer: Comparison of theory and measurements. *Aerosol Science and Technology, 43*(*11*), 1075–1083. https://doi.org/10.1080/02786820903095484.

Lee, S. Y., Widiyastuti, W., Tajima, N., Iskandar, F., & Okuyama, K. (2009). Measurement of the effective density of both spherical aggregated and ordered porous aerosol particles using mobility- and mass-analyzers. *Aerosol Science and Technology, 43*(*2*), 136–144. https://doi.org/10.1080/02786820802530524.

Liao, B.-X., Tseng, N.-C., & Tsai, C.-J. (2017). The accuracy of the aerosol particle mass analyzer for nanoparticle classification. *Aerosol Science and Technology, 52*(*1*), 19–29. https://doi.org/10.1080/02786826.2017.1370532.

Lin, G.-Y., Liao, B.-X., Tzeng, N.-J., Chen, C.-W., Uang, S.-N., Chen, S.-C., ... Tsai, C.-J. (2014). The effect of nanoparticle convection-diffusion loss on the transfer function of an aerosol particle mass analyzer. *Aerosol Science and Technology, 48*(*6*), 583–592. https://doi.org/10.1080/02786826.2014.902027.

Malloy, Q. G. J., Nakao, S., Qi, L., Austin, R., Stothers, C., Hagino, H., & Cocker, D. R. (2009). Real-time aerosol density determination utilizing a modified scanning mobility particle sizer-aerosol particle mass analyzer system. *Aerosol Science and Technology, 43*(*7*), 673–678. https://doi.org/10.1080/02786820902832960.

Mulholland, G. W., Zhou, L., Zachariah, M. R., Heinson, W. R., Chakrabarti, A., & Sorensen, C. (2013). Light scattering shape diagnostics for nano-agglomerates. *Aerosol Science and Technology, 47*(*5*), 520–529. https://doi.org/10.1080/02786826.2013.767435.

Olfert, J., & Collings, N. (2005). New method for particle mass classification-the couette centrifugal particle mass analyzer. *Journal of Aerosol Science, 36*(*11*), 1338–1352. https://doi.org/10.1016/j.jaerosci.2005.03.006.

Pavlis, N. K., Holmes, S. A., Kenyon, S. C., & Factor, J. K. (2008). The development and evaluation of the earth gravitational model 2008 (egm2008). *Journal of Geophysical Research: Solid Earth, 117*(*B4*).

Scheckman, J. H., McMurry, P. H., & Pratsinis, S. E. (2009). Rapid characterization of agglomerate aerosols by in situ mass-mobility measurements. *Langmuir, 25*(*14*), 8248–8254. https://doi.org/10.1021/la900441e.

Sinclair, D., Countess, R. J., Liu, B. Y. H., & Pui, D. Y. H. (1976). Experimental verification of diffusion battery theory. *Journal of the Air Pollution Control Association, 26*(*7*), 661–663. https://doi.org/10.1080/00022470.1976.10470299.

SINCLAIR, D. (1972). A portable diffusion battery. *American Industrial Hygiene Association Journal, 33*(*11*), 729–735. https://doi.org/10.1080/0002889728506738.

Tajima, N., Sakurai, H., Fukushima, N., & Ehara, K. (2013). Design considerations and performance evaluation of a compact aerosol particle mass analyzer. *Aerosol Science and Technology, 47*(*10*), 1152–1162. https://doi.org/10.1080/02786826.2013.827323.

van Zon, R., & Cohen, E. G. D. (2003). Stationary and transient work-fluctuation theorems for a dragged brownian particle. *Physical Review E, 67*(*4*), 046102. https://doi.org/10.1103/physreve.67.046102.

Wang, S. C., & Flagan, R. C. (1990). Scanning electrical mobility spectrometer. *Aerosol Science and Technology, 13*(*2*), 230–240. https://doi.org/10.1080/02786829008959441.

Wiedensohler, A. (1988). An approximation of the bipolar charge distribution for particles in the submicron size range. *Journal of Aerosol Science, 19*(*3*), 387–389. https://doi.org/10.1016/0021-8502(88)90278-9.

Wong, C.-S., Goree, J., Haralson, Z., & Liu, B. (2017). Strongly coupled plasmas obey the fluctuation theorem for entropy production. *Nature Physics, 14*(*1*), 21–24. https://doi.org/10.1038/nphys4253.

Wong, C.-S., Goree, J., & Gopalakrishnan, R. (2018). Experimental demonstration that a free-falling aerosol particle obeys a fluctuation theorem. *Physical Review E, 97*(*5*), 050601. https://doi.org/10.1103/physreve.97.050601.